(Received 25 November 2025, Accepted 5 February 2026, Scheduled 19 March 2026)

Double Slabs of Magnetic Metamaterial for Improving the Efficiency of Wireless Power Transfer Systems

Noor F. Habib[1, 2, *], Mohammad S. Bayati[2], and Nasr Alkhafaji[1]

[1] *Department of Communication Engineering, Engineering Technical College of Al-Najaf Al-Furat Al-Awsat Technical University, Najaf, Iraq*
[2] *Department of Electrical Engineering, Faculty of Engineering, Razi University, Kermanshah, Iran*

ABSTRACT: This paper focuses on enhancing the efficiency of wireless power transfer (WPT) using metamaterials (MTMs) only in the transmitter section, without modifying the receiver section. Power transfer efficiency (PTE) is the ratio of the actual power to the load resistance R_{load} that is transmitted to the load to the maximum available power at the source, V_s. Enhancing the PTE of a WPT system is essential, given the wide range of WPT applications. Magnetic MTMs can significantly increase PTE. This research proposes a structure for the transmitter (Tx) coil and receiver (Rx) coil, incorporating the MTM slab, in a WPT system to enhance efficiency. The MTM was fabricated on a thin FR-4 substrate and positioned in front of and behind the Tx coil. Full-wave simulations show a clear improvement in coupling after adding the MTM plate. The transmission coefficient S_{21} is increased by 0.4 when the MTM is placed in front of the Tx coil. When the two plates of the MTM were inserted, the S_{21} improved by 0.2 compared to a single slab due to dielectric losses. In all cases, the magnetic field became more distributed and focused on the receiver side after the addition of the MTMs. The power transfer efficiency reaches 53.3% with double-layer MTMs at 12 MHz and a distance of 35 mm. Finally, the results of the measurements and simulations showed acceptable agreement, indicating that the proposed method is effective in overcoming reduced efficiency issues. The proposed design is suitable for various electronic applications, such as multiple-device charging pads.

1. INTRODUCTION

The need for WPT has increased because the wires used today have many limitations and can be replaced with wireless power transfer. Convenient charging, wireless power transfer WPT systems own considerable promise for a variety of applications, such as sensor networks [1], consumer electronics [2], robotics [3], electric cars [4], and biological implants [5]. PTE is a system's ability to transmit power to the receiver. However, as the transfer distance increases, the PTE of the WPT system drops precipitously due to magnetic field divergence in under-coupled regions. Researchers suggested several methods to enhance PTE, including frequency tracking [6], impedance matching [7], relay resonators [8], and magnetic-field shaping to improve the coupling between Tx and Rx coils [9]. To enhance the coupling between (Tx) and (Rx) coils, several researchers have proposed using MTMs to regulate magnetic fields in WPT systems, thereby improving efficiency. MTMs have unique characteristics not found in natural materials [10–12]. They have been utilized in several fields, including absorbers, antennas, and biosensors [13–15]. This sophisticated material can manipulate electromagnetic waves, making it an optimal choice for improving efficiency and extending the transfer distance in WPT systems [16–18]. The exceptional characteristics of MTMs enable the design of structures that can bend, reflect, and absorb electromagnetic waves, thereby meeting the needs of WPT applications [19]. Ongoing research in this domain shows that MTMs will significantly enhance the capabilities of the WPT technique [20]. Diverse MTM configurations, including superconducting MTMs, reconfigurable MTMs, and laterally positioned MTMs, have been incorporated with WPT systems [21–23]. Flexible MTMs have been extensively utilized in various applications, including energy harvesting, electromagnetic wave absorption, and mechanical MTMs [24–26]. In [27], a compact WPT structure that integrates deep learning and a reconfigurable metasurface is proposed to enable smart power routing. The utilization of the MTM between the Tx and Rx terminates the sharp decline of the PTE in the traditional inductive coupling [28]. The following articles [29–33] addressed the role of MTMs in enhancing the performance and efficiency of WPT systems by mitigating the negative propagation properties of both μ and ϵ.

Figures 1(a) and (b) explain the distribution of the magnetic field with/without MTM.

In this article, we propose an MTM slab with resonance coils for Tx and Rx to find the best location of the MTM plate using a sequence of steps, in front of Tx, behind it, and double plates, with the first one in front of the Tx and the other one behind it, and study their effect on the PTE and the distribution of the magnetic field in the transmitter and receiver sides, respectively.

* Corresponding author: Noor Fadhel Habib (noor.habib@atu.edu.iq).

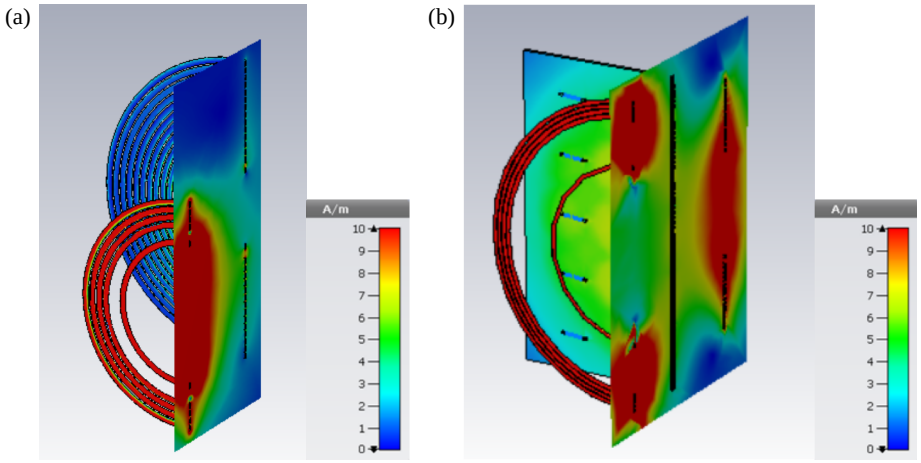

FIGURE 1. The WPT system, (a) the magnetic field without MTM, (b) with MTM.

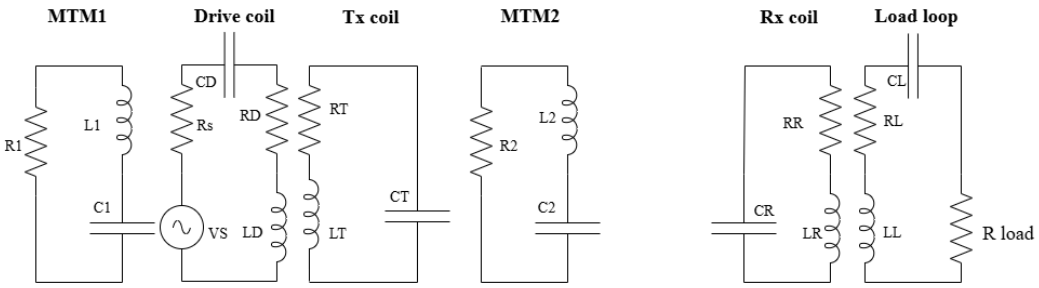

FIGURE 2. The RLC circuit model represents the Tx, Rx coils, and MTM.

2. THE EQUIVALENT CIRCUIT OF THE PROPOSED WPT WITH AND WITHOUT THE METAMATERIAL

The objective of the proposed design is to determine the optimal location for the MTM plate and enhance the PTE using one or two MTM plates. In the first case, one MTM slab is placed near the transmitter coil to focus the magnetic field and efficiently transmit it to the receiver. In the second case, double layers of MTMs are used, one opposite the Tx coil and the other behind it, to reduce magnetic-field leakage and enhance efficiency. Fig. 2 represents the equivalent circuit of the proposed design for both cases. The circle loops, magnetic resonance coils, and MTM slabs can be modeled by a series RLC as shown in Fig. 2. The Tx and Rx coils with MTM are characterized by an RLC model circuit. Driver coil is described as R_D, L_D, and C_D, while the MTM slab is defined as R_1, R_2, L_1, L_2, and C_1, C_2. The receiver coil is described as R_R, L_R, and C_R, the load loop is defined as R_L, L_L, and C_L.

Figure 2 illustrates the equivalent circuit for all wireless power transmission system designs employed in this study. A graphical depiction of the equivalent circuit describes the adopted WPT analysis situations. This model, shown in Fig. 2, is used to determine the equivalent relation and solve the system. Fig. 1(a), without MTMs, is a simple WPT that applies Kirchhoff's principles, enabling us to derive the equations for the system's voltage and current, as demonstrated below. The coupling effects among the source, Tx, Rx, and load coils are neglected to facilitate calculations while still accurately representing the system's main interactions.

$$\begin{bmatrix} V_S \\ 0 \\ 0 \\ 0 \end{bmatrix} = \begin{bmatrix} Z_D & j\omega M_{DT} & 0 & 0 \\ j\omega M_{DT} & Z_T & j\omega M_{TR} & 0 \\ 0 & j\omega M_{TR} & Z_R & j\omega M_{RL} \\ 0 & 0 & j\omega M_{RL} & Z_L \end{bmatrix} \begin{bmatrix} I_D \\ I_T \\ I_R \\ I_L \end{bmatrix} \tag{1}$$

$$Z_D = R_S + R_D + j\omega L_D + \frac{1}{j\omega C_D} \tag{1a}$$

$$Z_T = R_T + j\omega L_T + \frac{1}{j\omega C_T} \tag{1b}$$

$$Z_R = R_R + j\omega L_R + \frac{1}{j\omega C_R} \tag{1c}$$

$$Z_L = R_{Load} + R_L + j\omega L_L + \frac{1}{j\omega C_L} \tag{1d}$$

I_D, I_T, I_R, and I_L refer to the currents in the drive coil, Tx coil, Rx coil, and load loop, respectively. The matrix Equation (1) is

solved for the voltage across $Rload$, as shown in Equation (2).

$$\frac{V_{Load}}{V_{Source}} = \frac{(j\omega)^3 \cdot M_{DT}M_{TR}M_{RL}R_{Load}}{\left(Z_DZ_TZ_RZ_L + \omega^2\left(M_{DT}^2Z_RZ_L + M_{TR}^2Z_DZ_L + M_{RL}^2Z_DZ_T\right)\right) + \omega^4M_{DT}^2M_{RL}^2} \tag{2}$$

In the following analysis, we will examine a four-coil magnetically coupled resonant wireless power transfer system utilizing metamaterials, as illustrated in Fig. 1(b). Applying Kirchhoff's laws enables us to obtain the matrices for the voltages and currents of each loop, as shown in Equation (3).

$$\begin{bmatrix} 0 \\ V_S \\ 0 \\ 0 \\ 0 \\ 0 \end{bmatrix} = \begin{bmatrix} Z_1 & j\omega M_{1D} & 0 & 0 & 0 & 0 \\ j\omega M_{1D} & Z_D & j\omega M_{DT} & 0 & 0 & 0 \\ 0 & j\omega M_{DT} & Z_T & j\omega M_{T2} & 0 & 0 \\ 0 & 0 & j\omega M_{T2} & Z_2 & j\omega M_{2R} & 0 \\ 0 & 0 & 0 & j\omega M_{2R} & Z_R & j\omega M_{RL} \\ 0 & 0 & 0 & 0 & j\omega M_{RL} & Z_L \end{bmatrix} \begin{bmatrix} I_1 \\ I_D \\ I_T \\ I_2 \\ I_R \\ I_L \end{bmatrix} \tag{3}$$

$$Z_1 = R_1 + j\omega L_1 + \frac{1}{j\omega C_1} \tag{3a}$$

$$Z_2 = R_2 + j\omega L_2 + \frac{1}{j\omega C_2} \tag{3b}$$

I_1 and I_2 refer to the currents in MTM1 and MTM2, respectively. The matrix Equation (3) is solved for the voltage across R_{load}, as shown in Equation (4).

$$\frac{V_{Load}}{V_{Source}} = \frac{(j\omega)^5 \cdot M_{1D}M_{DT}M_{T2}M_{2R}M_{RL} \cdot R_{Load}}{\left(M_{1D}^2M_{T2}^2M_{RL}^2\omega^6 + A\omega^4 + B\omega^2 + Z_1Z_DZ_TZ_2Z_RZ_L\right)} \tag{4}$$

$$A = M_{1D}^2\left(M_{RL}^2Z_2Z_T + M_{2R}^2Z_TZ_L + M_{T2}^2Z_LZ_R\right) + M_{T2}^2M_{RL}^2Z_1Z_D + M_{DT}^2Z_1\left(M_{RL}^2Z_2 + M_{2R}^2Z_L\right) \tag{4a}$$

$$B = M_{1D}^2Z_TZ_2Z_RZ_L + M_{DT}^2Z_1Z_2Z_RZ_L + M_{T2}^2Z_1Z_DZ_LZ_R + M_{2R}^2Z_1Z_DZ_TZ_L + M_{RL}^2Z_1Z_DZ_2Z_T \tag{4b}$$

Assuming that the generator and load are conjugate matched to the reference impedance of the system, the efficiency of the WPT system can be determined from Equation (5), where the po and pi are the output and input power. In practical design, coil design and spacing are optimized using an electromagnetic simulation program (CST Studio Suite), while the analytical model is used to explain observed trends and validate physical intuition.

$$PTE = \frac{po}{pi} = 2\frac{V_{Load}}{V_{Source}}\sqrt{\left(\frac{R_{Source}}{R_{Load}}\right)} = |S_{21}|^2 \tag{5}$$

The matrix of the MTM inclusive was mentioned in Equation (3). The system is reduced to the baseline case by setting the mutual coupling terms M_{1D}, M_{T2}, and M_{2R} to zero values. In this state, the currents across the MTM impedances (Z_1 and Z_2) vanish, and the system reverts to the conventional 4-resonator configuration of the MTM structure. Then, Equation (4) is simplified to the baseline formulation in Equation (2).

3. THE DESIGN PROCEDURE AND THE SIMULATION RESULTS

Figure 3 illustrates the proposed approach of the WPT system, which includes a feed source coil, a transmitting coil, the MTM, a receiving coil, and a load coil.

The source coil is contained within a transmitter coil, and the Tx is constructed from 4 turns with a spiral shape. The inner diameter of the driving coil is 56 mm, and the capacitor of the Tx coil is 67 pF, which is connected in series with the resistance ($= 50\,\Omega$). The load coil, combined with the receiver coil, has 14 turns. The inner diameter of the Rx coil is 32 mm and is placed 35 mm above the Tx coil. A capacitor (9 pF) was inserted in series with a resistance load ($100\,\Omega$) to achieve the desired resonance frequency. For the MTM to be employed in practical situations and to prevent ohmic losses, it must be designed as compactly as feasible with finite unit cells. Furthermore, it is crucial to remember that MTM is excited by a source in the near field, rather than by a plane wave. Thus, we achieved an overall external dimension of $168.6 \times 168.6\,\text{mm}^2$ by realizing a 5×5 unit cell of the MTM. These features are sufficient to improve the mutual coupling coefficient between the Tx and Rx. Each unit cell consists of a 5-turn spiral resonator with a 0.84 mm radius. In the first case, Tx and Rx coils are studied without using MTM. In the second case, the MTM is added in front of the transmitter, and then two layers of MTM are used, one in front of the transmitter and the other behind it. The most critical dimensions of the proposed design are listed in Table 1.

4. THE ANALYSIS OF THE DESIGN MTM WITH TX AND RX COILS

The particular unit cell design is a resonant tank with the metallic traces acting as inductors (L) and the gaps as capacitors (C). The out-of-phase response of the surface currents at the resonant frequency of 12 MHz results in an effective negative permeability, which is a property of a split-ring-like resonator. The MTM slab is in close proximity to the coils near resonance, where it interacts with the coils' near field and enhances the evanescent waves, which would otherwise die off. This serious increase in the magnetic flux density between the Tx and Rx coils leads to a significant enhancement in the Power Transfer Efficiency (PTE). The MTM structure uses magnetic-field manipulation by passing the flux lines through its high-permeability/negative-refraction region. It concentrates the magnetic field, minimizes leakage, and enhances the transmission coefficient (S_{21}). This modulation is manifested in our 5th-order system matrix (Equation (3)) in which the MTM res-

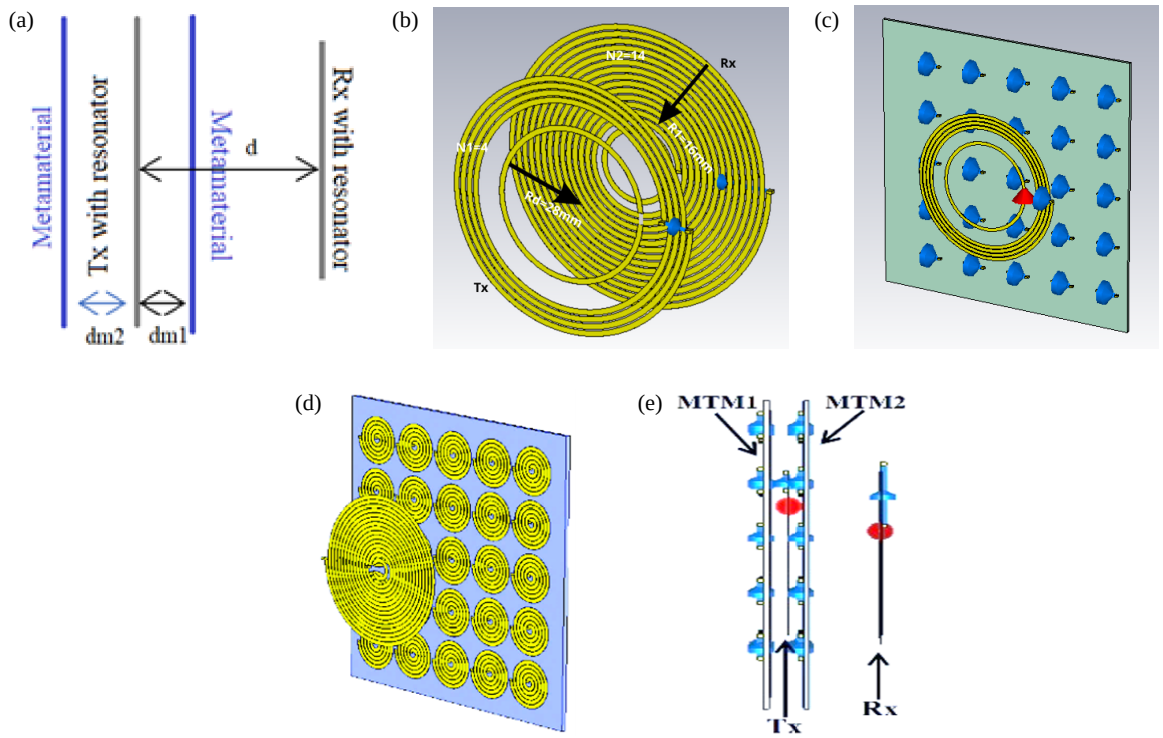

FIGURE 3. WPT with resonator and double-sided MTM, (a) the layout shows the distances between the MTM1 and MTM2, (b) a side view of two coils without MTM, (c) a back view of the MTM, (d) a front view of the MTM, (e) a bottom view of two coils with double plates of the MTM.

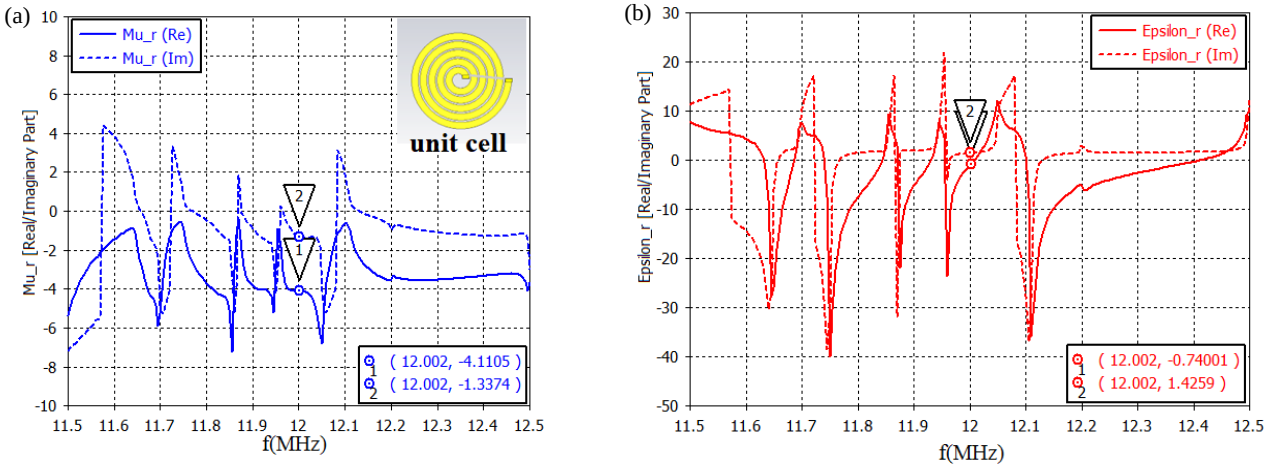

FIGURE 4. The unit-cell design with the variation of μ, and ε, (a) the real and imaginary parts of μ, (b) the real and imaginary parts of ε.

onators (Z_1, Z_2) result in new coupling paths (M_{1D}, M_{T2}, M_{2R}), which are absent in the baseline system. This mathematical paradigm demonstrates that the MTM is an active modulator of the magnetic connection, not a passive one. Fig. 4(a) and Fig. 4(b) illustrate the unit cell design and the real and imaginary parts of the permeability and permittivity, respectively. The parametric study was conducted to determine the optimal values of w (the width of the wire) and g (the gap between turns) as shown in Figs. 5(a), and (b). The simulations were performed with CST software to examine the magnetic resonance WPT system with MTM. Two ports of a discrete type are utilized to simulate the drive loop and load loop. In numerous practical applications, the distance between the transmitter (Tx) and receiver (Rx) in a WPT system is not readily available, so we examine several distances and calculate their efficiencies. Fig. 6 shows the simulation results for S_{21} between the transmitting and receiving coils without MTM at various distances.

The MTM was added at the midpoint between the transmitter and receiver coils to enhance the coupling between them, thereby increasing the system's efficiency. Fig. 7(a) shows the transmission coefficient as a function of the distance between the Tx and Rx when an MTM plate is added. The distance between the transmitter and MTM is also studied, and the obtained

TABLE 1. Summary of the most critical dimensions of the proposed design.

Parameter	Value	Description
w	2 mm	The width of the wire
g	0.5 mm	The gap between turns
N_1	4	The number of turns in Tx
N_2	14	The number of turns in Rx
N_3	5	The number of turns in the MTM unit cell
R_d	28 mm	The radius of the driver
R_1	16 mm	The radius of the load coil
R_3	0.85 mm	The radius of the unit cell
d	35 mm	The distance between Tx and Rx
d_n	9 mm	The front distance between the Tx coil and MTM when using one layer
d_z	28 mm	The back distance between the Tx and the MTM when using one layer
d_{m1}	14 mm	Front distance between the Tx and the MTM when using 2 layers
d_{m2}	20 mm	back distance between the Tx and the MTM when using 2 layers

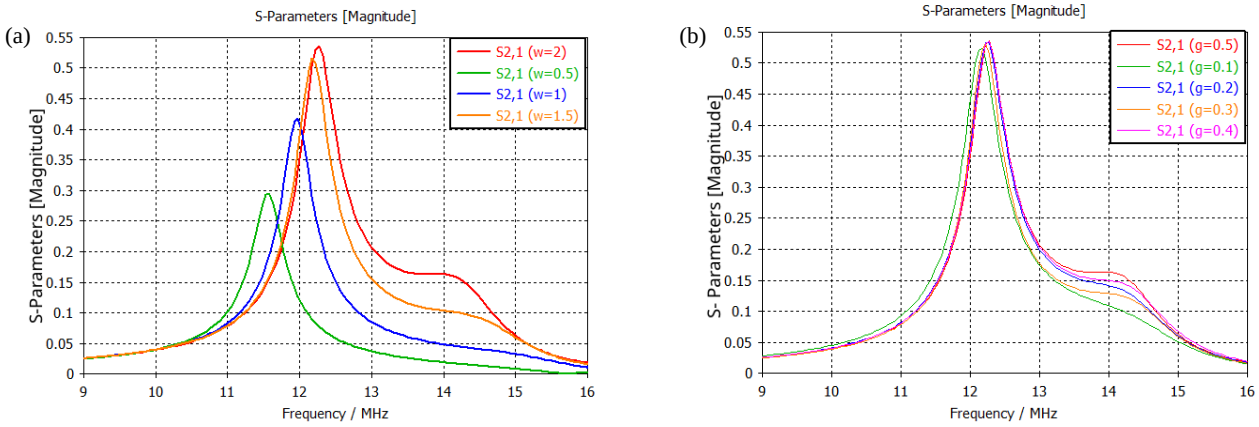

FIGURE 5. The parametric study of w and g, (a) study w, (b) study g.

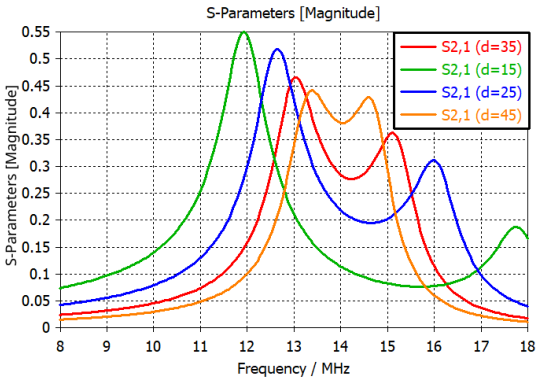

FIGURE 6. The S_{21} parameter of the Tx and Rx coils without MTM for several distances.

results demonstrate an improvement in S_{21} from 0.15 to 0.55, as shown in Fig. 7(b).

In the next step, we relocated the MTM plate to the backspace of the Tx coil to improve the magnetic field focus on the receiver coil. Fig. 8(a) explains the WPT system's response for various distances between the transmitter and receiver. The S_{21} increased at 11 MHz and 12 MHz after moving the MTM slab behind the Tx coil, thereby increasing the PTE at these two frequencies. The back distance between the MTM and transmitter coil is represented as d_z (in the case of one layer of the MTM) and studied from 8 to 28 mm. The obtained results showed an increase in S_{21} from 0.55 to 0.56 as explained in Fig. 8(b). To reduce magnetic field leakage and improve efficiency by increasing the power transmitted from the Tx coil to the Rx coil, we added a second layer of MTM, one opposite the Tx coil and the other behind it. Fig. 9(a) shows the transmission coefficient as a function of distance. The front distance (d_{m1}) and the back distance (d_{m2}) were also studied, and it was observed that a d_{m1} of 14 mm yielded a high transmission coefficient; therefore, S_{21} increased from 0.56 to 0.73, as shown in Fig. 9(b). The back distance (d_{m2}) is also optimized for several values, and a d_{m2} of 20 mm yields a significant improvement in the S_{21} parameter compared to other values, as shown in Fig. 9(c). Fig. 10 shows the "focusing" effect of the magnetic-field distribution. These plots clearly reveal that the MTM reshapes the field lines, concentrating the magnetic flux toward the receiver coil. This increased flux density raises the mutual inductance M_{RL}, as predicted by Equations (2) and (4). The magnetic

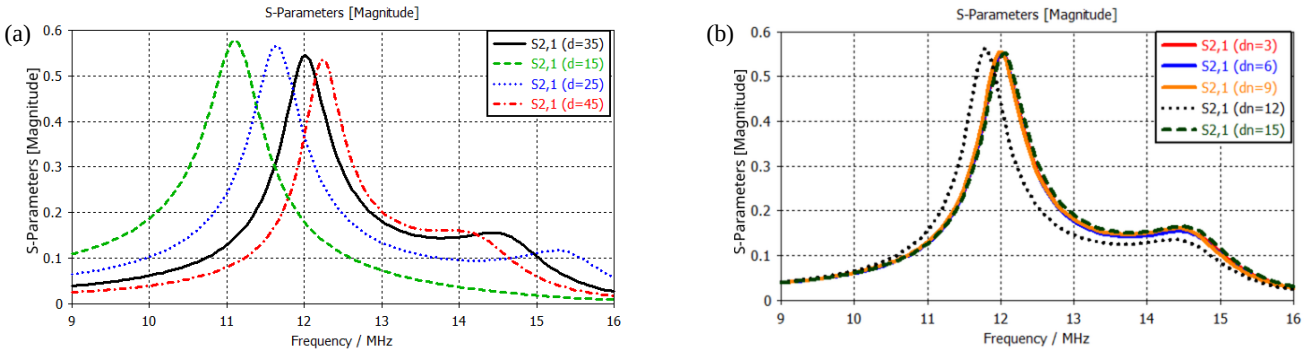

FIGURE 7. The S_{21} parameter, when adding the MTM (a) at different distances between Tx and Rx, (b) studies the distance between the MTM and the Tx.

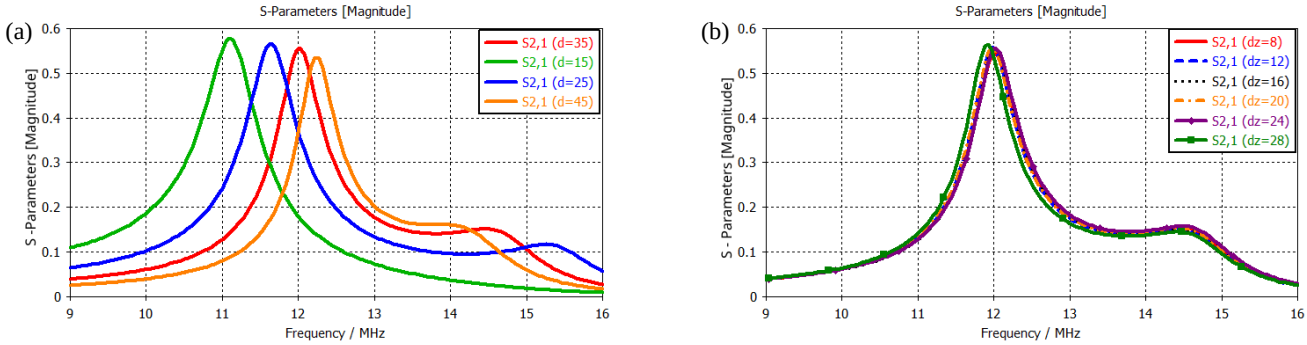

FIGURE 8. The S_{21} parameter, when placing the MTM behind the Tx, (a) study the distance between the coils, (b) study the distance between the Tx and the MTM.

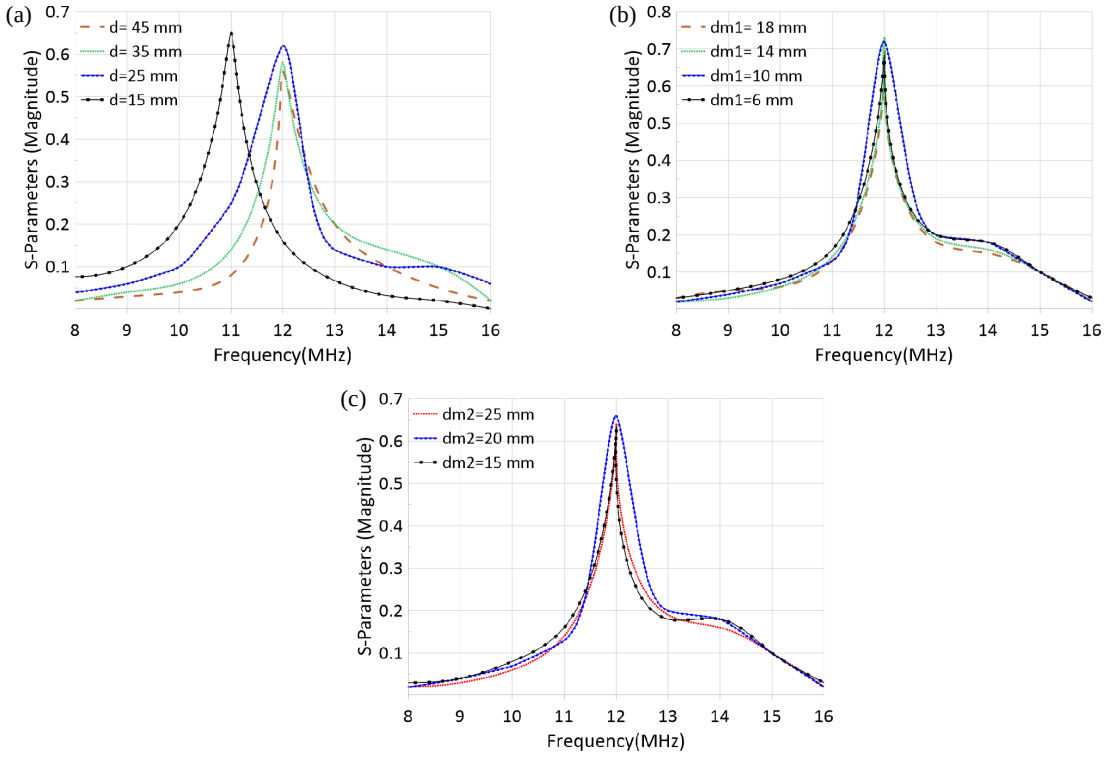

FIGURE 9. The S_{21} parameter when adding two plates of the MTM, (a) for various separated distances between the Tx and Rx, (b) for various d_{m1}, (c) for various d_{m2}.

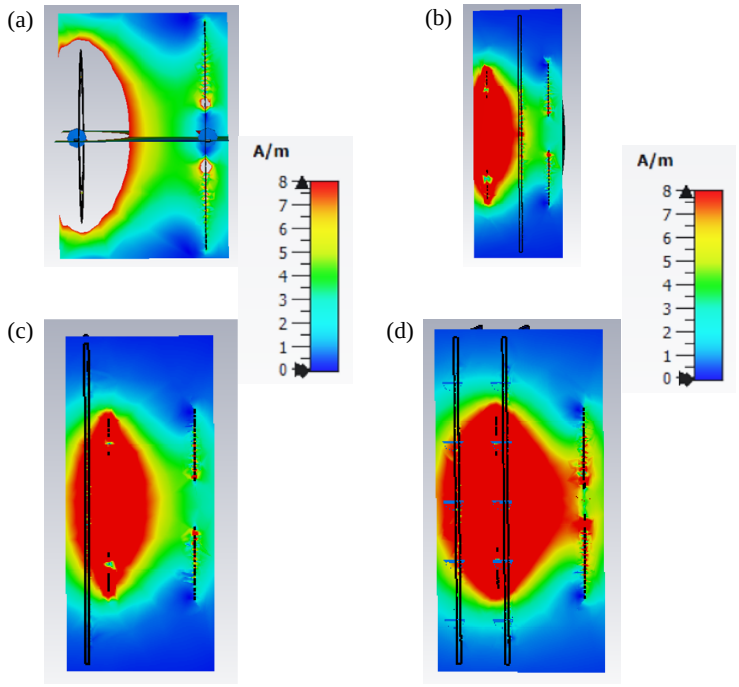

FIGURE 10. The distribution of the magnetic field, (a) two coils without MTM, (b) the MTM in front of the Tx coil, (c) the MTM behind the Tx coil, (d) with double layers of the MTM.

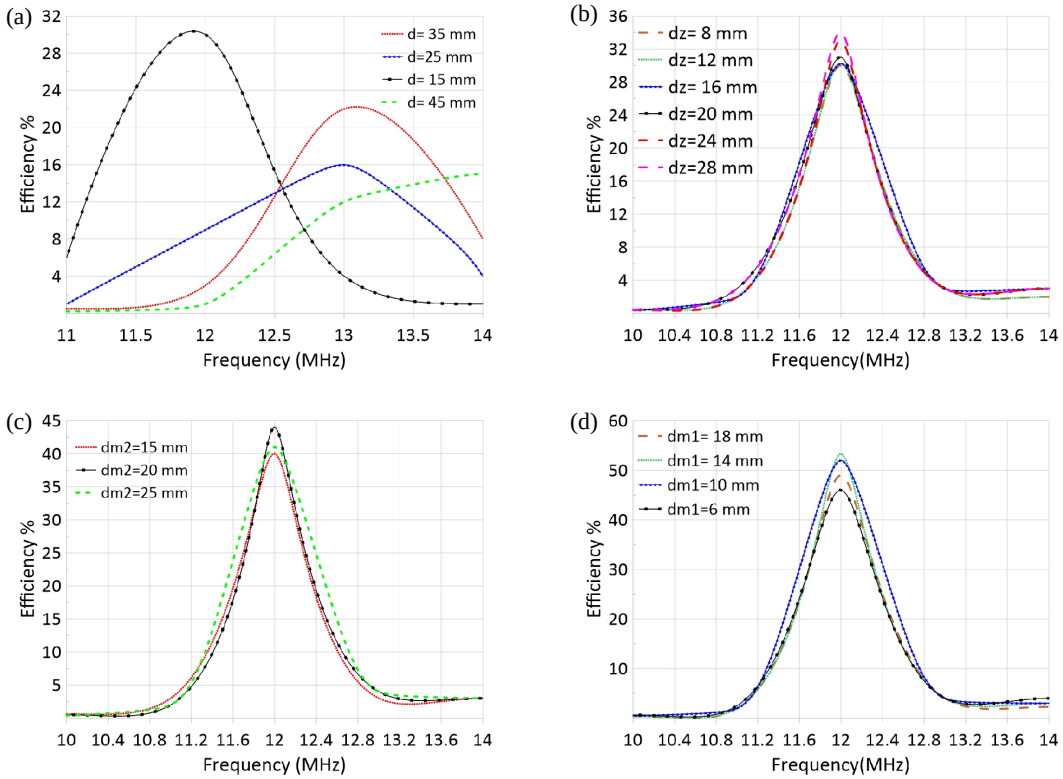

FIGURE 11. The efficiency of the proposed design, (a) only two coils without MTM, (b) the MTM in front of the transmitter coil, (c) the MTM behind the transmitter coil, (d) with two slabs of the MTMs, one in front of the Tx and the other behind it.

field distribution, when two coils are used without MTM, is shown in Fig. 10(a). Fig. 10(b) represents the magnetic field when the MTM is moved in front of the coils, Fig. 10(c) when the MTM is placed behind the coils, and Fig. 10(d) when two plates of the MTM are used. The transmission efficiency of the WPT system was evaluated under various cases, as shown in Fig. 11. Initially, the simulated resonator coils were used without the MTM, achieving an efficiency of 30% at 12 MHz,

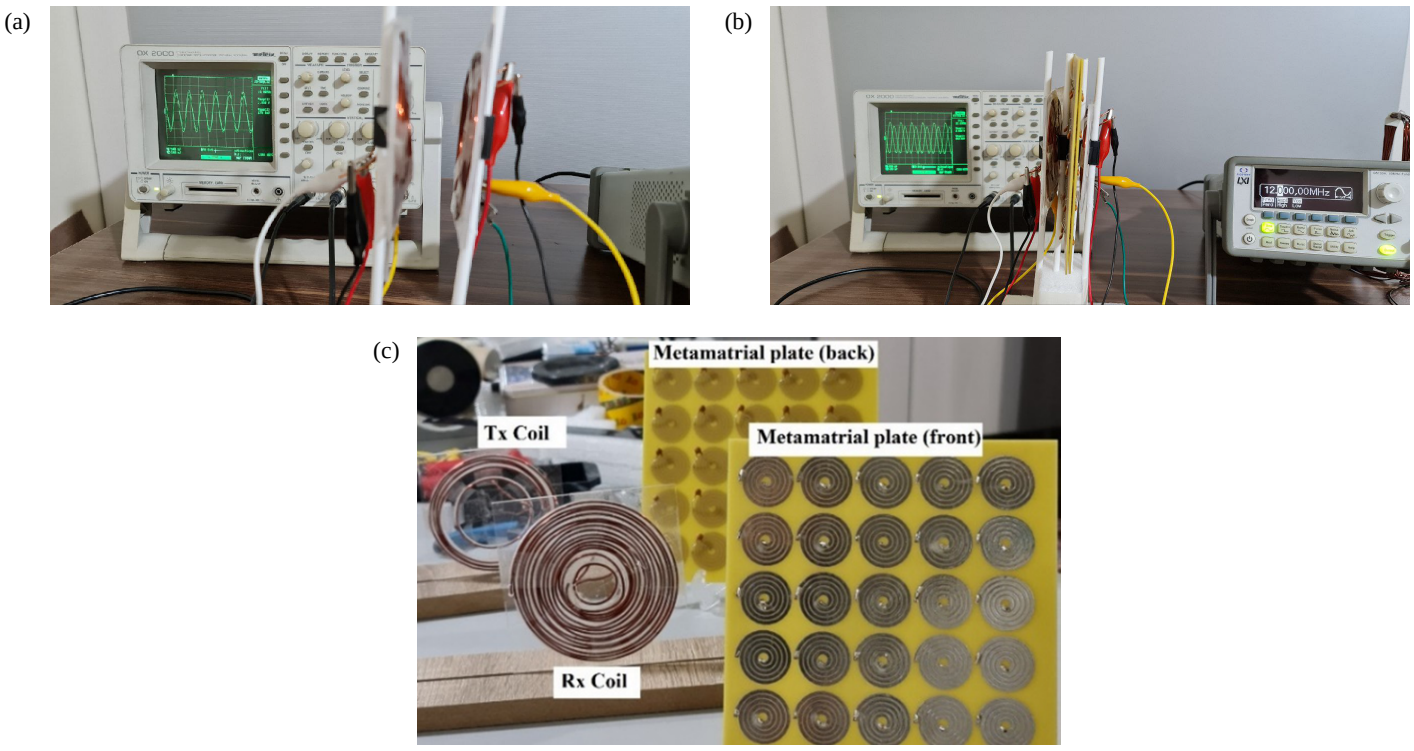

FIGURE 12. The fabrication and measurement process for the suggested design, (a) Tx and Rx coils without MTM, (b) Tx and Rx coils with one slab of MTM, (c) with two slabs of MTM.

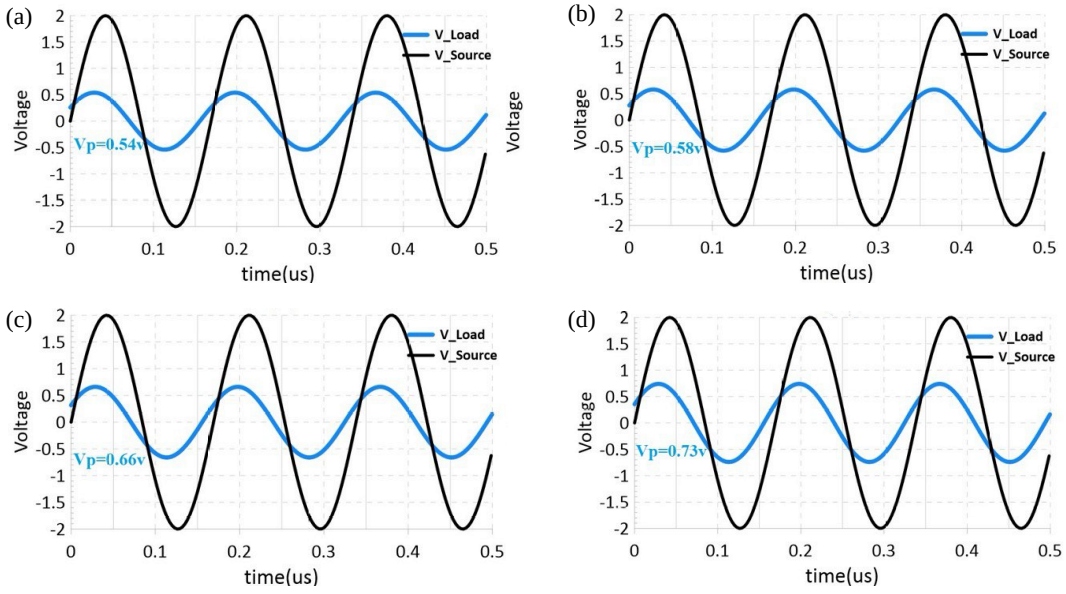

FIGURE 13. The improvement of V_{source} and V_{load} for different cases, (a) $V_p = 0.54$, (b) $V_p = 0.58$, (c) $V_p = 0.66$ v, (d) $V_p = 0.73$ v.

as illustrated in Fig. 11(a). In the second case, the MTM layer was inserted in front of the Tx coil, yielding an efficiency of 35%, as shown in Fig. 11(b). In the third case, the MTM plate was moved to the back space behind the Tx coil, and the efficiency was measured at 44% for $d_{m2} = 20$ mm (where d_{m2} is the back distance between the MTM and Tx coils), as shown in Fig. 11(c). Finally, efficiency improved when another MTM slab was added, reaching 53.3% at $d_{m1} = 14$ mm (where d_{m1} is the front distance between the MTM and Tx coil), as shown in Fig. 11(d). According to S_{21} values with and without the MTM, as reviewed in all previous instances, the resonance frequency remains well-matched, and the power transferred from the Tx to the Rx coil is increased. Consequently, the observed enhancement in S_{21} cannot be attributed to a reduction in mismatch loss; it is instead a direct result of improved magnetic flux linkage. Table 2 shows the comparison between the sim-

TABLE 2. The comparison between the simulated results of this work and other researches on WPT with MTM.

Ref.	Location of the MTM slab	The number of MTM slabs	The number of unit cells	The resonance frequency	Efficiency
[30]	In front of Tx	One layer	7×7	6.78 MHz	41.7%
[32]	In the middle	One layer	5×5	12 MHz	40%
[33]	In the middle	One layer	5×5	13.5 MHz	50.5%
This work	One in front of Tx and the other behind it	Two layers	5×5	12 MHz	53.3%

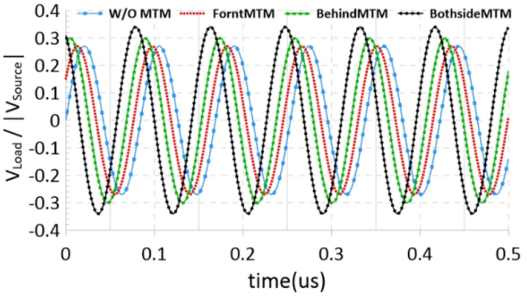

FIGURE 14. Comparison of the measurement for the output voltage between various positions of the MTM.

ulated results of this work and other researches on WPT with MTM.

5. THE FABRICATION PROCESS OF THE PROPOSED DESIGN

To validate the effectiveness of the suggested design, we fabricate the Tx and Rx coils with MTM, as shown in Fig. 12. The materials used in fabrication are FR-4 (dielectric constant of 4.3 and the thickness = 1.5 mm) for the MTM design and pure copper for the Tx and Rx coils and MTM unit cells (the thickness of the copper 0.035 mm). Two capacitors are added to the Tx and Rx coils, and 25 capacitors are added to the (5×5) MTM to tune the resonance frequency, and the distance between adjacent cells is 25 mm. The measurement results showed agreement with the simulated ones. This study can be instrumental in the development of WPT applications, such as biomedical implants and consumer devices. Fig. 13 shows the V_{source} and V_{load} for four cases. The peak of V_{load} is increasing from 0.45 V to 0.73 V, which means enhancing the voltage transfer efficiency by 0.35%, and it is also noticed that the V source remains consistent at 5 V (peak voltage), which is important because the increase in V_{load} is a direct result of increasing V_{load}/V_{source}. Fig. 14 compares the measurement and simulation results.

6. CONCLUSION

This article presents the study and analysis of a WPT system with MTM to improve transmission efficiency. The simulated results showed that using the magnetic MTM can enhance the efficiency of the WPT system. Efficiency increases from 30% to 53.3% when the MTM plate is used. We study multiple sequences with different procedures at the resonance frequency of 12 MHz with a separation distance of 35 mm between the transmitter (Tx) and receiver (Rx). The transmission coefficient improved when inserting the MTM(s) in front of the Tx coil and in the back space behind the coils. The leakage of the magnetic field is also reduced and increased in focus toward the receiver side when MTM slabs are added. The proposed design was fabricated, and the simulation and measurement results are in agreement, indicating that the design's theoretical basis is effective. The current prototype is best suited for desktop-sized applications, such as multiple-device charging pads or small home appliances.

REFERENCES

[1] Hong, Y.-W. P., T.-C. Hsu, and P. Chennakesavula, "Wireless power transfer for distributed estimation in wireless passive sensor networks," *IEEE Transactions on Signal Processing*, Vol. 64, No. 20, 5382–5395, Oct. 2016.

[2] Ullah, M. A., R. Keshavarz, M. Abolhasan, J. Lipman, K. P. Esselle, and N. Shariati, "A review on antenna technologies for ambient RF energy harvesting and wireless power transfer: Designs, challenges and applications," *IEEE Access*, Vol. 10, 17 231–17 267, 2022.

[3] Kim, S.-M., J.-I. Moon, I.-K. Cho, J.-H. Yoon, W.-J. Byun, and H.-C. Choi, "Advanced power control scheme in wireless power transmission for human protection from EM field," *IEEE Transactions on Microwave Theory and Techniques*, Vol. 63, No. 3, 847–856, Mar. 2015.

[4] Onar, O. C., S. L. Campbell, L. E. Seiber, C. P. White, M. S. Chinthavali, L. Tang, P. H. Chambon, B. Ozpineci, and D. E. Smith, "Oak ridge national laboratory wireless charging of electric vehicles — CRADA report," ORNL/TM-2016/296, Oak Ridge National Laboratory, Oak Ridge, TN, USA, 2016.

[5] Xiao, C., K. Wei, D. Cheng, and Y. Liu, "Wireless charging system considering eddy current in cardiac pacemaker shell: Theoretical modeling, experiments, and safety simulations," *IEEE Transactions on Industrial Electronics*, Vol. 64, No. 5, 3978–3988, May 2017.

[6] Kim, N. Y., K. Y. Kim, Y.-H. Ryu, J. Choi, D.-Z. Kim, C. Yoon, Y.-K. Park, and S. Kwon, "Automated adaptive frequency tracking system for efficient mid-range wireless power transfer via magnetic resonanc coupling," in *2012 42nd European Microwave Conference*, 221–224, Amsterdam, Netherlands, 2012.

[7] Beh, T. C., M. Kato, T. Imura, S. Oh, and Y. Hori, "Automated impedance matching system for robust wireless power transfer via magnetic resonance coupling," *IEEE Transactions on Industrial Electronics*, Vol. 60, No. 9, 3689–3698, Sep. 2013.

[8] Zhong, W. X., C. Zhang, X. Liu, and S. Y. R. Hui, "A methodology for making a three-coil wireless power transfer system more energy efficient than a two-coil counterpart for extended transfer distance," *IEEE Transactions on Power Electronics*, Vol. 30, No. 2, 933–942, Feb. 2015.

[9] Zhu, Q., M. Su, Y. Sun, W. Tang, and A. P. Hu, "Field orientation based on current amplitude and phase angle control for wireless power transfer," *IEEE Transactions on Industrial Electronics*, Vol. 65, No. 6, 4758–4770, Jun. 2018.

[10] Wu, K., J.-J. Liu, Y.-j. Ding, W. Wang, B. Liang, and J.-C. Cheng, "Metamaterial-based real-time communication with high information density by multipath twisting of acoustic wave," *Nature Communications*, Vol. 13, No. 1, 5171, Sep. 2022.

[11] Ha, D. T., B. S. Tung, B. X. Khuyen, T. S. Pham, N. T. Tung, N. H. Tung, N. T. Hoa, V. D. Lam, H. Zheng, L. Chen, and Y. Lee, "Dual-band, polarization-insensitive, ultrathin and flexible metamaterial absorber based on high-order magnetic resonance," *Photonics*, Vol. 8, No. 12, 574, 2021.

[12] Sahandabadi, S., S. V. A.-D. Makki, and S. Alirezaee, "Design of a reflectarray antenna using graphene and epsilon-near-zero metamaterials in terahertz band," *Progress In Electromagnetics Research Letters*, Vol. 89, 113–119, 2020.

[13] Wu, G.-B., J. Y. Dai, K. M. Shum, K. F. Chan, Q. Cheng, T. J. Cui, and C. H. Chan, "A universal metasurface antenna to manipulate all fundamental characteristics of electromagnetic waves," *Nature Communications*, Vol. 14, No. 1, 5155, 2023.

[14] Van Long, L., D. N. Dung, P. T. Son, N. T. Tung, V. T. H. Hanh, D. T. Ha, D. T. Chi, B. S. Tung, B. X. Khuyen, and V. D. Lam, "Robust reversion of dual-band polarization conversion and absorption based on flexible metamaterial," *Journal of the Physical Society of Japan*, Vol. 92, No. 2, 024801, 2023.

[15] Patel, S. K., J. Parmar, V. Sorathiya, T. K. Nguyen, and V. Dhasarathan, "Tunable infrared metamaterial-based biosensor for detection of hemoglobin and urine using phase change material," *Scientific Reports*, Vol. 11, No. 1, 7101, Mar. 2021.

[16] Smirnov, P., E. Koreshin, G. Baranov, and P. Kapitanova, "Self-tuning approach for metasurface-based resonators for one-to-many wireless power transfer," *Journal of Applied Physics*, Vol. 134, No. 8, 084901, Aug. 2023.

[17] Habib, N. F., M. S. Bayati, and N. Alkhafaji, "Improving the performance of a wireless power transfer with misalignment using magnetic resonators coil and metamaterial slabs," *Progress In Electromagnetics Research C*, Vol. 160, 48–55, 2025.

[18] Younesiraad, H. and M. Bemani, "Analysis of coupling between magnetic dipoles enhanced by metasurfaces for wireless power transfer efficiency improvement," *Scientific Reports*, Vol. 8, No. 1, 14865, 2018.

[19] Hiep, L. T. H., B. X. Khuyen, B. S. Tung, Q. M. Ngo, V. D. Lam, and T. S. Pham, "Flexible magnetic metasurface with defect cavity for wireless power transfer system," *Materials*, Vol. 15, No. 19, 6583, 2022.

[20] Rong, C., L. Yan, L. Li, Y. Li, and M. Liu, "A review of metamaterials in wireless power transfer," *Materials*, Vol. 16, No. 17, 6008, 2023.

[21] Bui, H. N., T. S. Pham, J.-S. Kim, and J.-W. Lee, "Field-focused reconfigurable magnetic metamaterial for wireless power transfer and propulsion of an untethered microrobot," *Journal of Magnetism and Magnetic Materials*, Vol. 494, 165778, Jan. 2020.

[22] Lu, C., X. Huang, X. Tao, C. Rong, and M. Liu, "Comprehensive analysis of side-placed metamaterials in wireless power transfer system," *IEEE Access*, Vol. 8, 152 900–152 908, 2020.

[23] Hou, Y., X. Wang, Y. Wang, Y. Hu, Y. He, and Z. Yan, "Analysis of wireless power transfer using superconducting metamaterials," *IEEE Transactions on Applied Superconductivity*, Vol. 29, No. 2, 1–5, Mar. 2019.

[24] Jiang, S., X. Liu, J. Liu, D. Ye, Y. Duan, K. Li, Z. Yin, and Y. A. Huang, "Flexible metamaterial electronics," *Advanced Materials*, Vol. 34, No. 52, 2200070, 2022.

[25] Bertoldi, K., V. Vitelli, J. Christensen, and M. V. Hecke, "Flexible mechanical metamaterials," *Nature Reviews Materials*, Vol. 2, No. 11, 1–11, Oct. 2017.

[26] Anjali, M., R. Sahoo, L. Stephen, C. V. Krishnamurthy, and V. Subramanian, "Flexible bandwidth-enhanced metamaterial absorbers with epoxy/graphene nanoplatelets-silver nanowire polymer composites as substrates," *Composites Science and Technology*, Vol. 249, 110492, Apr. 2024.

[27] Li, W., Q. Yu, J. H. Qiu, and J. Qi, "Intelligent wireless power transfer via a 2-bit compact reconfigurable transmissive-metasurface-based router," *Nature Communications*, Vol. 15, No. 1, 2807, 2024.

[28] Yusri, M. S., M. H. Misran, M. A. M. Said, M. A. Othman, A. Salleh, R. A. Ramlee, S. K. A. Rahim, and M. Z. Idris, "Optimizing wireless power transfer efficiency at 13.56 MHz using double negative metamaterials," *Progress In Electromagnetics Research B*, Vol. 111, 125–133, 2025.

[29] Shaw, T., B. Mandal, G. Samanta, T. Voigt, D. Mitra, and R. Augustine, "Rotation insensitive implantable wireless power transfer system for medical devices using metamaterial-polarization converter," *Scientific Reports*, Vol. 14, No. 1, 19688, 2024.

[30] Cho, Y., S. Lee, D.-H. Kim, H. Kim, C. Song, S. Kong, J. Park, C. Seo, and J. Kim, "Thin hybrid metamaterial slab with negative and zero permeability for high efficiency and low electromagnetic field in wireless power transfer systems," *IEEE Transactions on Electromagnetic Compatibility*, Vol. 60, No. 4, 1001–1009, 2018.

[31] Wang, X., Y. Wang, Y. Hu, Y. He, and Z. Yan, "Analysis of wireless power transfer using superconducting metamaterials," *IEEE Transactions on Applied Superconductivity*, Vol. 29, No. 2, 1–5, 2019.

[32] Lazzoni, V., D. Brizi, and A. Monorchio, "Spatial filtering magnetic metasurface for misalignment robustness enhancement in wireless power transfer applications," *Scientific Reports*, Vol. 13, No. 1, 560, 2023.

[33] Hiep, L. T. H., H. N. Bui, B. S. Tung, V. D. Lam, B. X. Khuyen, and T. S. Pham, "Enhanced efficiency of magnetic resonant wireless power transfer system using rollable and foldable metasurface based on polyimide substrate," *Applied Physics A*, Vol. 130, No. 7, 521, 2024.